ASTRONOMY & ASTROPHYSICS
SUPPLEMENT SERIES
Astron. Astrophys. Suppl. Ser. **106**, 339-348 (1994)

Deep photometry in the core of the open cluster NGC 5606*,**

R.A. Vázquez[1], G. Baume[2], A. Feinstein[1] and P. Prado[3]

[1] Observatorio Astronómico de La Plata, Paseo del Bosque S/N, 1900 La Plata, Argentina and PROFOEG–CONICET
[2] Observatorio Astronómico de La Plata, Paseo del Bosque S/N, 1900 La Plata, Argentina
[3] University of Toronto Southern Observatory, Las Campanas, Chile

Received January; accepted March 14, 1994

Abstract. — The center of the open cluster NGC 5606 has been re–observed with broad band *UBVRI* CCD photometry. Up to $V = 18.5$ likely cluster members are found underlining a sharp but not so populated cluster sequence. With this new photometry the cluster distance modulus is stated in $V_0 - M_v = 11.90$ ($d = 2400$ pc). The mean colour excess reaches the value $\langle E_{B-V} \rangle = 0.51$. The age of the cluster from the isochrone fitting is between $6.3\,10^6$ and $7\,10^6$ y. Surprisingly enough there are not many stars found below $V = 15.5$ in spite of the fact that we are observing the very core of the cluster. This lack of faint cluster stars produces in turn a flat slope for the cluster mass spectrum. In this respect our computation yields $x = 1.09$ far enough of $x = 1.35$ which is assumed to be the slope characterizing the mass spectrum of galactic stars.

Key words: open cluster: NGC 5606 — stars: mass function — HR diagram

1. Introduction

The open cluster NGC 5606 = C1424–594 consists of a small size grouping of early–type stars surrounded by a few members up to a distance of 10 arcmin from it. It is situated in a low absorption zone of the Galaxy in $l = 314°$ (Feinstein 1994) and its distance would indicate that it is placed in the inner side of Sagittarius arm. Its low absorption pattern remind us the neighbour region of Carina clusters. NGC 5606 has not been much investigated and the readers are referred to Vázquez & Feinstein (1991a) for a brief review on its characteristics and earlier investigations. The most notorious part of NGC 5606 is the center itself which has a size of 2×2 arcminutes and within which it is possible to see five bright stars forming a very compact group. Our first investigation in the region of NGC 5606 covered an area larger than the present one, about 10×10 arcminutes, and our photometry on that occasion was done up to $V = 13.5$.

We re–included the cluster in our program on small open clusters but this time we concentrate our effort in doing deep CCD photometry in the very core of the cluster. Looking for fainter members than in our first investigation we attempt to increase the photometric basis for a more precise determination of the distance, age and reddening of this cluster. We are aware that today there exists an increasing need of learning about the slope of the mass spectrum in this type of open clusters. Then, we will carry out an analysis of the faint main sequence stars.

2. Observations

CCD *UBVRI* (Cousins system) observations of 156 stars in NGC 5606 were carried out in the night of April 9-10 1992 using the 60 cm telescope of the University of Toronto Southern Observatory, Las Campanas, Chile and a PM 512 × 512 METACHROME chip UV coated. Observations were obtained under good weather conditions on a photometric night (about 1.3″ seeing). The chip (4 arcminutes on a side) has been positioned in the center of the cluster. Figure 1 is a finding chart of the field covered by the present investigation. We have identified all cluster member stars (see Sect. 3) using filled circles and the size of the symbols approximately represents the star visual magnitude. Bias frames and dome flats were used to remove instrumental signatures. Point spread function (PSF) fitting using the DAOPHOT (Stetson 1987) version within IRAF was employed to derive instrumental colours and magnitudes. In a given filter frames of identical exposure time were combined into one in order to improve the statistics for the faintest stars. All the calculations were done on the Ultrix-cluster at the Astronomy Institutes of the Bonn University (Germany). During the process of

Send offprint requests to: Dr. A. Feinstein
*Based on observations collected at The University of Toronto Southern Observatory, Las Campanas, Chile
**Table 3 is also available in electronic form: see the Editorial in A&AS 1994, Vol. 103, No. 1

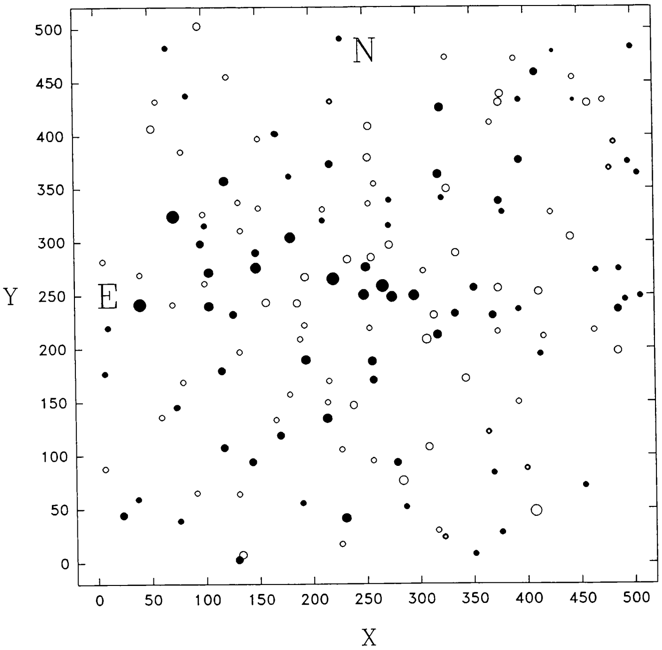

Fig. 1. Finding chart of the core of NGC 5606. The size of the circles approximately represents the value of the V magnitudes. Filled circles denote likely and possible cluster members. Open circles are for non members (see Sect. 3)

making the PSF, we did not notice a change along the frame. Usually we employed over 15 well isolated stars to construct a single PSF valid on the entire frame. Details of the exposures in the *UBVRI* filters can be found in Table 1. Several stars in the frames have previous *UBVRI* photoelectric photometry done by us (Vázquez & Feinstein 1991a). We use this photometry to calibrate each frame to get final colours and magnitudes. Atmospheric extinction correction was apllied using extinction coefficients from Grothues & Gochermann (1992). So we do not use a self-calibrating method. A comparison of the PSF magnitudes and photoelectric magnitudes shown in Table 2 reveals that the mean differences are meaningless but the standard deviations are a bit high, however. Such high standard deviations could originate in the fact that our calibration stars are not exactly true "standards" and some of the faintest ones only have a single observation. Nonetheless, the large number of stars adopted as "standards" let us consider that the observations adequately match up to the standard system. For completeness we show in Fig. 2a-e the array of error values based upon Poisson statistics for each filter against the V magnitude. Table 3 lists the adopted sequential number # and the identification number V&F (V&F = Vázquez & Feinstein, 1991a), X and Y star coordinates and observed magnitudes and colours. A colon (:) suggests *combined* errors from 0.07 to 0.10 and the double colon (::) indicates errors larger than 0.10. We inform that in our first paper on NGC 5606 we misprinted the identification numbers of stars 13 and 14.

Table 1. A detail of scientific frames and exposure times

Filter	Exposure times[sec] *Long*	*Mid*	*Short*
U	600 (2)	200 (2)	60 (2)
B	300 (2)	120 (2)	50 (2)
V	100 (2)	50 (2)	12 (1)
R	80 (1)	40 (2)	15 (1)
I	50 (2)	25 (2)	10 (1)

Note: the number of used frames are given in bracketts

Table 2. Comparison with photoelectric photometry in the sense PSF photometry minus photoelectric photometry

<ΔV> σ	<Δ(B-V)> σ	<Δ($U-B$)> σ	<Δ(V-R)> σ	<Δ(V-I)> σ
0.002	0.008	0.009	-0.013	-0.000
0.039	0.033	0.039	0.023	0.043

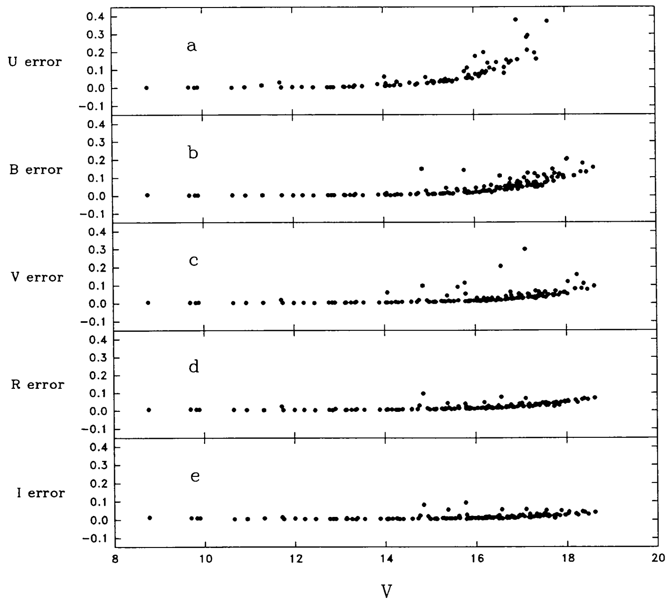

Fig. 2. a-e. The array of errors from Poisson statistics as a function of the V magnitude for the *UBVRI* filters

3. Analysis of the data

Unfortunately the long exposure frames in the U filter were not long enough to reach the same magnitude depth as the *BVRI* frames do. So, there is a number of stars without any U magnitudes measured. In what follows and just to give reliable results we have estimated that "good values" are those whose *combined* errors in observed magnitudes and colours are smaller than 0.07.

In the absence of proper motion study in the cluster region we are compelled to base our analysis onto photometric arguments. We state that likely cluster members are those stars simultaneously having reconcilable positions in colour–colour and colour–magnitude diagrams respectively. Some stars, in spite of their ambiguous positions could not definitively be rejected as likely cluster members. For this kind of stars we use the designation of possible members (pm).

Figure 3 presents the $(U-B)$ vs $(B-V)$ colour-colour diagram where the intrinsic colour line from Schmidt-Kaler (1982) valid for stars of luminosity Class V was shifted by $E_{B-V} = 0.51$ mag. Figures 4, 5, 6 and 7 show the plots of V values against $(B-V)$, $(U-B)$, $(V-R)$ and $(V-I)$ indices respectively. With them and Fig. 3 we will proceed to evaluate memberships in the cluster.

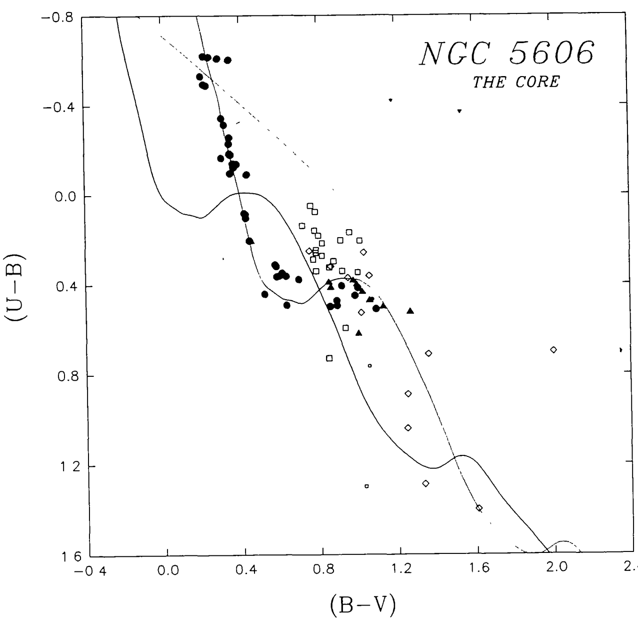

Fig. 3. Colour-colour diagram. Symbols: filled circles are for likely members; filled triangles are for possible cluster members; open squares identify the curious stars group discussed in Sect. 3; inverted triangles give the placement of the two very blue and reddened stars; open diamonds are foreground stars. Note: small symbols always are used to indicate errors larger than 0.07. The lines are the Schmidt-Kaler ZAMS (1982). One of them is shifted by $< E(B-V) > = 0.51$. Also the path of the reddening line is shown

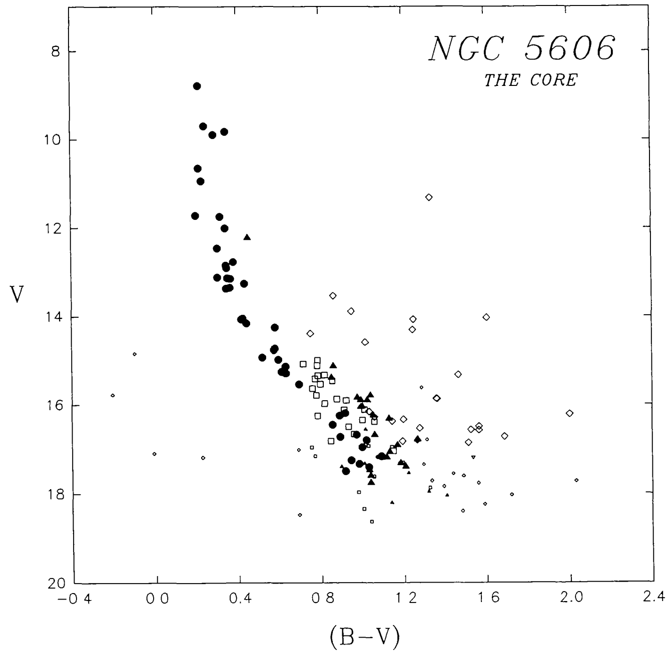

Fig. 4. The V vs $(B-V)$ diagram. Symbols as in Fig. 3

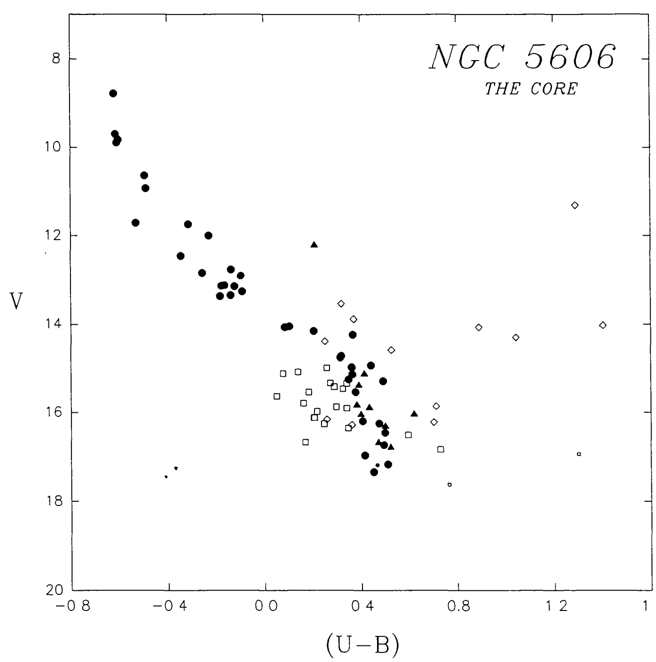

Fig. 5. The V vs $(U-B)$ diagram. Symbols as in Fig. 3

A simultaneous inspection of these five diagrams reveals the existence of a sharp and less scattered OB–type star sequence (filled circles) as well as some stars that (according to their colours) are of late A-, and early F-types. Notice that differential reddening is not notorious although late B-type stars seem to be a bit affected. Both groups constitute the open cluster NGC 5606. Between them, a gap is seen in the colour-magnitude diagrams extending from $V = 15$ to $V = 16.5$ approximately. This gap is filled up by another star group (empty squares; small squares indicate large errors) that has the following peculiarity: in Fig. 3 its components seem to be reddened B-type stars without any apparent relation to the cluster but, surprisingly enough, they situate comfortably well along the cluster main sequence in all the colour-magnitude diagrams. It could be possible for these stars

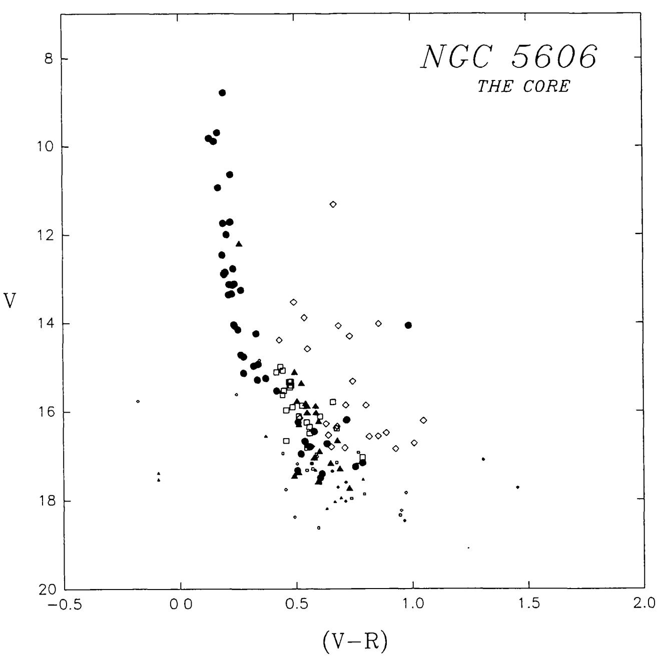

Fig. 6. The V vs $(V-R)$ diagram. Symbols as in Fig. 3

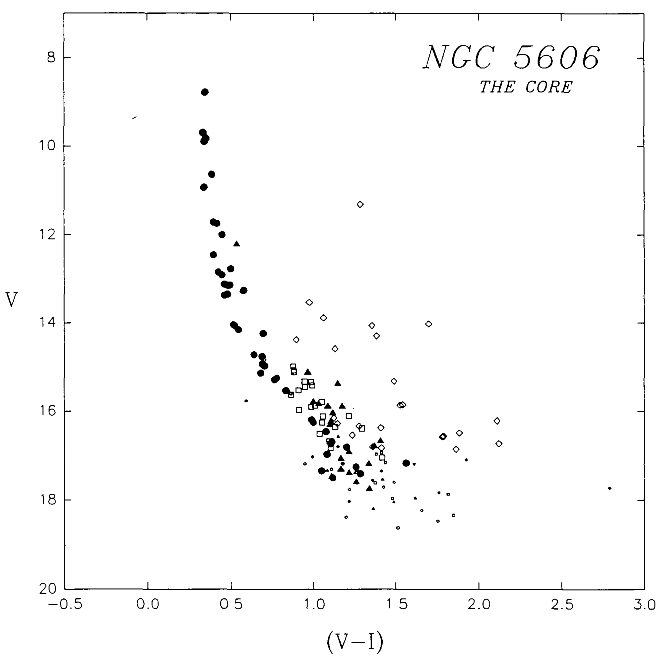

Fig. 7. The V vs $(V-I)$ diagram. Symbols as in Fig. 3

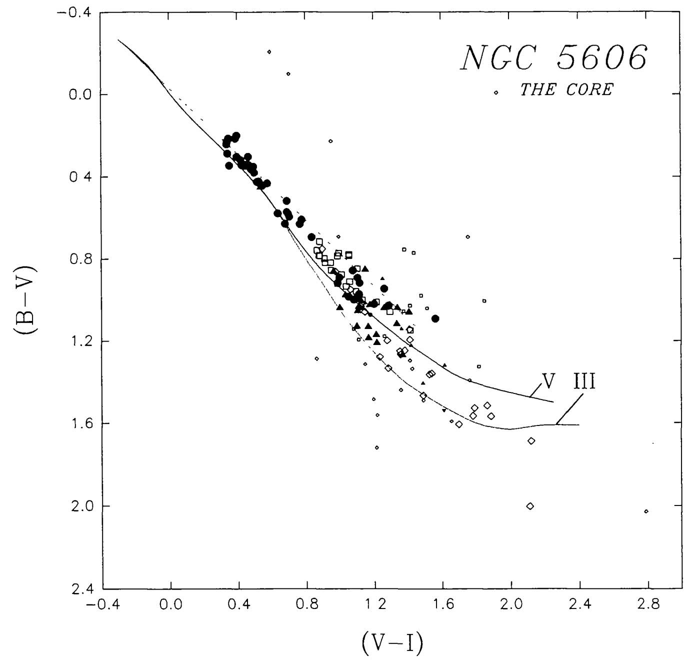

Fig. 8. The $(B-V)$ vs $(V-I)$ diagram. Symbols as in Fig. 3. Dotted straight line indicates the path of the reddening line for an 0-type star. Solid lines are the intrinsic lines for luminosity Classes III and V

to be reddenend background B-type stars as their observed colours and magnitudes allow this solution. However, the bend observed in the V vs $(V-R)$ diagram is like that observed in clusters with pre-main sequence stars. It is possible for them to be pre-main sequence stars too. In that case they should show, at least, some excess E_{V-I} in the diagram of Fig. 8, but they do not. In our opinion, further IR observations and spectroscopy are needed to explain these stars. Two very reddened blue, but also very faint stars (#56 and #93), indicated with inverted triangles, are seen through the cluster core. These two stars, despite their errors, have no chance to be physically related to the cluster. Obvious foreground stars (empty diamonds; small diamonds indicate large errors) are easily segregated from cluster stars as they are brighter than expected when comparing their positions in all the five diagrams. There still remain some stars (filled triangles) situated in the region comprised by $0.7 < (B-V) < 1.2$ and $0.30 < (U-B) < 0.60$ in the colour-colour diagram. In Figs. 5, 6 and 7 they join another star sample lacking $(U-B)$ indices with positions that also are compatible with the one corresponding to possible cluster members. Additionaly, most of these stars do have significant $(U-B)$ and $(B-V)$ errors, which makes their placement on the diagrams rather precarious. So, as we lack precise photometric arguments to reject these stars we retain them under the denomination of possible cluster members. One of these stars, #7 (V&F 57), had been rejected as cluster member in our first work but now we retain it as possible cluster member. The $(U-B)$ index of this star is a bit reddened and displaces it slightly in Fig. 5.

Like in our earlier work on this cluster we found that the reddening law behaves normally as shown in Fig. 8 that represents the plot of $(B-V)$ vs $(V-I)$ values. The lines of luminosity Classes V and III from Cousins (1978) are superimposed on the diagram along with the reddening line (straight line) for O–type stars derived by

Dean et al. (1978). Cluster members follow pretty well the path of this last line whose slope is $E_{V-I}/E_{B-V} = 1.244$.

Once the stars with some chance to become cluster members were selected we proceeded to derive intrinsic values. To do this we apply to the relations $E_{U-B}/E_{B-V} = 0.72 + 0.05\,E_{B-V}$ and $(U-B)_0 = 3.69\,(B-V)_0 + 0.03$ following Vázquez & Feinstein (1991b). Both these relations can only be used whith stars having unambiguous reddening solution. We computed a mean colour excess $\langle E_{B-V}\rangle = 0.51$ employing only the bluest and less scattered stars.

While for stars with unambiguous reddening, a solution in the CMD is clearly accessible to compute reliable individual E_{B-V} and E_{U-B} colour excesses there is no chance of making the same for stars without $(U-B)$ indices. For them we derived corrected $(B-V)_0$ indices using the mean value $\langle E_{B-V}\rangle = 0.51$. Assuming that the reddening law behaves normally we decided to estimate corrected magnitudes through the expression $V_0 = V - 3.1 \times E_{B-V}$. In Cols. 2 to 6 of Table 4 intrinsic quantities for likely and possible members are listed.

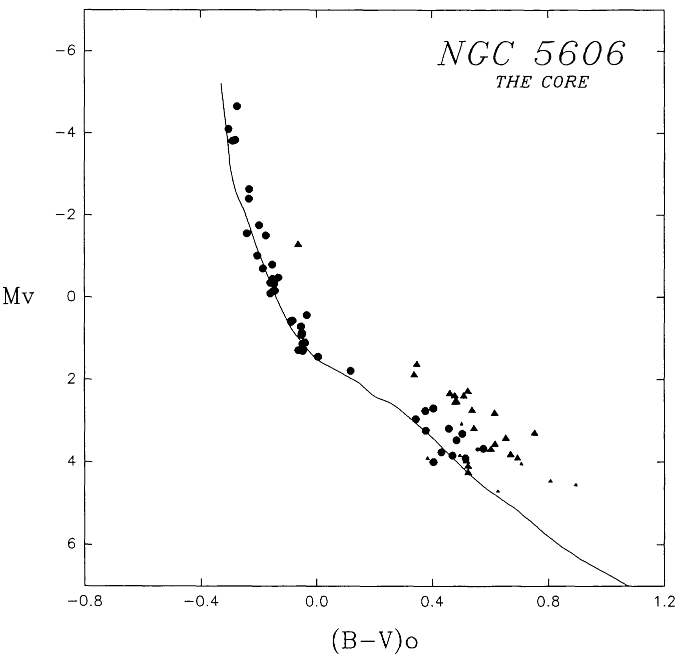

Fig. 9. The M_V vs $(B-V)_0$ diagram for likely and possible cluster members. Symbols as in Fig. 3. the Schmidt-Kaler ZAMS (1982) is fitted to a distance modulus $V_0 - M_V = 11.90$

4. Distance and age

The fitting procedure of Schmidt–Kaler's ZAMS (1982) was employed to derive the distance modulus of NGC 5606. The best fitting in both the V_0 vs $(B-V)_0$ and V_0 vs $(U-B)_0$ planes, was achieved for a distance modulus $V_0 - M_V = 11.90 \pm 0.20$ corresponding to a distance $d = 2400$ pc. To save space we only show the fit in the M_V vs $(B-V)_0$ diagram of Fig. 9. Absolute magnitudes obtained with this distance modulus are shown in the Col. 7 of Table 4. The fact that we were able to find faint cluster members allow us to get a better definition of the cluster lower main sequence which in turn improves the estimation of the distance. The distance modulus also can be estimated through the relation between spectral types and absolute magnitudes given by Schmidt–Kaler (1982). By employing the five stars of Table 4 having a known spectral classification we computed a spectrophotometric distance modulus $V_0 - M_V = 11.85 \pm 0.50$. Both distance moduli are close enough but we prefer the photometric one which is less affected by the influence of the high scatter in the absolute magnitudes of B-type stars.

The age of NGC 5606 is determined with the aid of the isochrones of Maeder & Meynet (1988) computed from a set of evolutionary tracks with mass loss and overshooting. The $(B-V)_0$ and M_V values from Cols. 8 and 9 in Table 4 were converted into $\log T_{\rm eff}$ and $\log L/L_\odot$ by means of the relations from Schmidt–Kaler (1982). The procedure is explained in Vázquez et al (1994). The resulting HR diagram of NGC 5606 is shown in Fig. 10. No chance to achieve a single isochrone fitting for the whole sample of stars is apparent from the figure. Therefore we just employed the four brightest stars in order to estimate the cluster age. According to the placement and the way we handled the data the age is situated between 6.3 and 7 million years. It is important to keep in mind that the cluster age depends on the values adopted in the transformations, the tracks used and the photometric errors.

5. Cluster mass spectrum

Let us consider from our CCD photometric data the stars up to $V = 18.5$ mag. to investigate the mass spectrum of the core of NGC 5606 and evaluate whether the slope of the frequency distribution of masses agrees or not with Salpeter's (1955) standard value $x = 1.35$. It has been a deal of controversy about the reliability of this value, however. Many authors report that the slope of the Initial Mass Function (IMF) of massive stars varies with the galactic radius (Burki 1978; Sagar et al. 1986; Garmany et al. 1982) though some other as Humphreys & McElroy (1984) do not find any change in the slope of the IMF within the Galaxy. In addition Conti (1992) shows that the slope of the IMF of massive stars is not only changing in our galaxy but also in the LMC. Actually, the concept of "standard" value in the case of the slope of the IMF does not seem to be appropriate.

The data sample to compute the slope of the cluster mass spectrum was drawn from Col. 10 of Table 4. We have computed the star masses transforming photometric data, M_V and $(B-V)_0$, into $\log L/L_\odot$ and $\log T_{\rm eff}$. With the aid of Maeder & Meynet (1988) tracks, we interpolated in order to get the initial stellar masses as

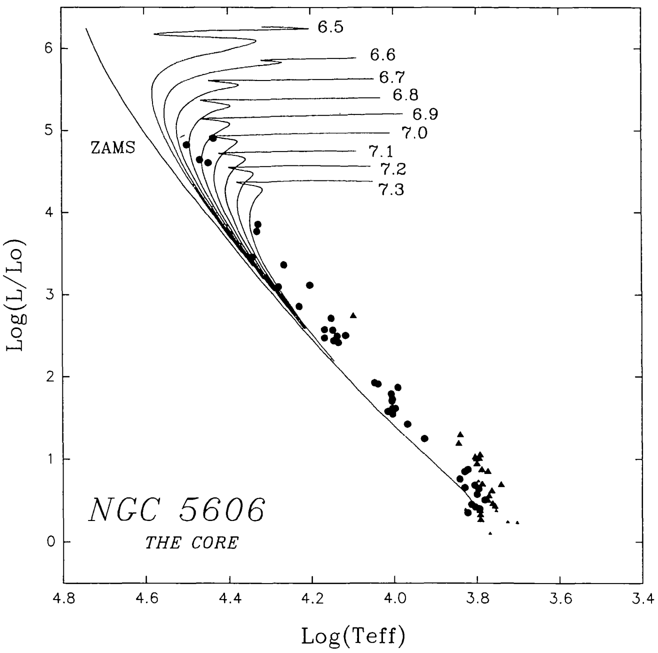

Fig. 10. The HR diagram of likely and possible cluster members. Symbols have the same meaning as in Fig. 3. Dotted lines are the isochrones of Maeder & Meynet (1988) computed with mass loss and overshooting. Numbers at the end of every lines indicate the log(age). The position of the theoretical ZAMS is shown

described in Vázquez et al. (1994). The mass range goes from nearly 1 $M_\odot$ to 30 $M_\odot$ approximately. In the computation of the mass spectrum given by the expression $\log(dN/d\log(M)) = -x\log M$, we have included likely and possible cluster members.

Table 5 lists mass bins, star counts (N) the Log$N$ and the logarithm of the mean mass Log$< M >$. The resulting slope $x = 1.09$ together with the standard deviation (SD) and the correlation coefficient (CC) are also shown. Stars having 1 $M_\odot$ correspond to $V = 17.8$ mag approximately where photometric errors become greater (see Fig. 2). It could be argued that incompleteness is affecting the lowest mass bin and hence the final result. Therefore we evaluated the influence of incompleteness by rejecting the lowest mass bin of Table 5 and performed a new calculation. The new result was $x = 1.04$ indicating that incompleteness is not playing a critical role. This evidence let us think that there is a real lack of faint stars in the cluster zone. On the other hand, using photometry alone (with standard errors of 0.02) for the computation of the slope of the mass spectrum can lead to fairly uncertain results. The most serious effects occur among massive stars as the errors on final masses can reach up to 60% according to our own estimations. To assess whether our result is dependent on the photometric data we re-calculated the slope x computing the star masses according to their spectral classification. We did not notice any remarkable change in the slope value so we retain the value in Table 5 as representative of the mass spectrum of the cluster core. The slope of the mass spectrum of the core of NGC 5606

Table 5. Cluster mass spectrum

Massbin	*N*	*LogN*	*Log < M >*
1-2	40	1.60	0.16
2-4	17	1.23	0.46
4-8	9	1.00	0.72
8-16	3	0.48	1.04
16-32	3	0.48	1.26
x =	1.09		
SD =	0.10		
CC =	0.77		

is rather flat, $x = 1.09$. Slopes so flat like this (or even flatter) have been reported to exist in many open clusters (Sagar et al. 1986). However, most of those slopes have been derived without having a precise knowledge on the number of faint stars not taken into account. In conclusion, those slopes are mainly related to the most massive stars. Our photometry goes deep down $V = 18.5$ mag. and hence we could expect that the incompleteness is affecting the number of stars below $V = 17.5$ and not above this limit. In our case the range covered to compute the mass spectrum is quite large and we are able to evaluate its particular pattern: there exists a notorious and real decreasing in the number of stars below $V = 15.5$ magnitudes. We do not extend this conclusion to the whole cluster as some mass segregation would miss a large fraction of the fainter stars, however.

Although being flat, the slope of the mass spectrum of NGC 5606 is adequately situated between the "normal" limits $x = 1.0$ in CygOB2 and $x = 1.3$ for the inner galactic field following the analysis by Conti (1992).

By counting stellar masses (Table 4) it results that the core of the cluster has a total observed mass of 250 $M_\odot$. We do not expect it changes too much if stars outside the center are included.

6. Concluding remarks

This new and deep photometry let us improve the distance as well as the mean reddening and cluster age in relation to earlier determinations.

New very faint likely and possible members have been found although some of them could be of a bit later type, say A- and F-types.

Colours and magnitudes for stars in the very compact grouping in the center of the cluster are now better determined as our measurements are free of light contamination from neighbours. The slope of the cluster mass spectrum is between the limits of normality but there exists a remarkable deficiency in the number of less massive cluster stars.

Acknowledgements. R.A.V. warmly thanks an invitation from Prof. Dr. W. Seggewiss to stay at the Astronomy Institutes of Bonn University (Germany) where part of this work has been made. He also thanks the generous collaboration of J.–M. Will and very specially the Institute's Director Prof. Dr. K. de Boer for his hospitality. Travel expenses and subsistence grant were provided by CONICET and the DAAD respectively. We are indebted to our careful referee Dr. J.-C. Mermilliod for his suggestions to improve this work and to Dr. Robert Garrison for the allocation of telescope time.

References

Burki G. 1977, A&AS 57, 135
Conti P.S. 1992, in IAU Symp 149 The Stellar Populations of Galaxies, eds. B. Barbuy & A. Renzini
Cousins A.W.J. 1978, Mon. Notes Astron. Soc. S. Afr. 37, 62
Dean J.F., Warren P.R. and Cousins A.W.J. 1978, MNRAS 183, 569
Feinstein A. 1994 (submitted to RMAA)
FitzGerald M.P., Luiken M., Maitzen H.M. & Moffat A.F.J. 1979, A&AS 37, 345
Garmany K.D., Conti P.S. & Chiosi C. 1982, ApJ 263, 777
Grothues H.-G. & Gochermann J. 1992, The Messenger No. 68, p. 43
Humphreys R.M. & McElroy D.B. 1984, ApJ 284, 565
Maeder A., Meynet G. 1988, A&AS 76, 411
Sagar R., Piskunov A.E., Myakutin V.I. & Joshi U.C. 1986, MNRAS 220,383
Schmidt-Kaler Th. 1982, in Landolt–Bornstein, Neue Series, VI/2b
Stetson P.B. 1987, PASP 99, 191
Vázquez R.A., Feinstein A. 1991a, A&AS 87, 383
Vázquez R.A., Feinstein A. 1991b, A&AS 90, 317
Vázquez R.A., Will J.–M., Feinstein A. & Prado P. 1994, in preparation

Table 3. Observed colours and magnitudes in NGC 5606

#	V&F	X	Y	V	U − B	B − V	V − R	V − I
100	15	220.97	265.16	8.776	-0.619	0.215	0.192	0.347
84	17	266.93	258.51	9.695	-0.615	0.243	0.165	0.336
81	1	41.11	241.30	9.823	-0.603	0.346	0.131	0.353
49	2	72.51	323.76	9.892	-0.610	0.288	0.150	0.341
5		249.39	250.21	10.649	-0.495	0.215	0.221	0.386
3	10	181.00	303.90	10.938	-0.490	0.228	0.167	0.340
43	29	407.61	47.55	11.318	1.289	1.333	0.666	1.285
157	18	275.41	248.05	11.716	-0.530 ::	0.200 ::	0.219	0.396
33	19	296.14	249.57	11.747	-0.315	0.318	0.189	0.418
55	12	148.54	275.65	11.996	-0.229	0.342	0.204	0.449
7	57	256.47	187.75	12.211	0.207	0.451	0.258	0.538
17	14	104.59	239.66	12.457	-0.344	0.304	0.185	0.396
19	6	119.79	357.26	12.767	-0.137	0.381	0.232	0.499
60	58	214.06	134.71	12.841	-0.257	0.344	0.198	0.425
27	59	194.89	189.64	12.906	-0.097	0.347	0.194	0.447
51	13	104.77	271.39	13.119	-0.165	0.303	0.237	0.462
9	56	317.79	212.41	13.132	-0.179	0.351	0.215	0.493
129	60	230.61	41.32	13.148	-0.123	0.365	0.229	0.481
34	9	321.21	425.58	13.255	-0.091	0.432	0.265	0.577
10	11	319.14	362.95	13.348	-0.140	0.363	0.224	0.479
101		251.28	276.11	13.369	-0.184	0.344	0.212	0.467
8		284.33	75.94	13.534	0.319	0.862	0.493	0.976
86		307.44	208.21	13.886	0.370	0.950	0.539	1.063
6		253.68	379.05	14.029	1.400	1.606	0.859	1.698
1		23.37	44.28	14.047	0.104	0.425	0.234	0.516
28		218.03	372.74	14.066	0.087	0.424	0.235	0.526
158		130.06	2.91	14.066	0.083	0.418	0.989 ::	
35		335.25	289.13	14.067	0.890	1.250	0.685	1.355
2		117.68	107.38	14.153	0.204	0.443	0.252	0.548
18		116.20	179.43	14.246	0.365	0.581	0.328	0.697
41		374.51	255.98	14.301	1.042	1.246	0.733	1.384
75		458.72	430.10	14.389	0.250	0.751	0.430	0.897
121		96.64	502.62	14.590	0.526	1.016	0.553	1.131
32		279.11	92.86	14.722	0.319	0.580	0.265	0.639
125		97.26	298.19	14.762	0.312	0.574	0.276	0.690
141		234.18	283.35	14.842 :		-0.098 ::	0.344 ::	0.704 ::
154		148.47	289.78	14.937	0.442	0.519	0.339	0.691
11		334.34	232.35	14.975	0.361	0.596	0.319	0.705
12		442.07	304.42	14.991	0.258	0.785	0.435	0.877
66		314.50	230.79	15.080	0.138	0.716	0.446	0.881
79		485.51	197.15	15.118	0.077	0.783	0.416	0.882
89		375.28	337.55	15.123	0.413	0.861	0.495	0.965
73		394.65	376.44	15.135	0.363	0.630	0.277	0.680
122		257.64	170.33	15.254	0.348	0.611	0.371	0.778
105		409.95	458.69	15.286	0.491	0.632	0.333	0.766
90		377.74	438.42	15.325		1.466	0.746	1.490
116		326.82	349.26	15.331	0.272	0.818	0.479	0.948
102		254.56	408.42	15.343	0.340	0.786	0.472	0.986
137		369.25	230.57	15.378	0.390	0.851	0.525	1.150 :
103		272.99	296.56	15.414	0.288	0.772	0.480	0.993
13		52.86	406.58	15.460	0.324	0.855	0.475	0.950
117		376.10	430.35	15.532	0.183	0.798	0.450	0.911
54		143.93	93.89	15.539	0.376	0.696	0.418	0.835
140		256.22	285.01	15.615 :		1.287 :	0.243 :	0.864 :

#	V&F	X	Y	V	U − B	B − V	V − R	V − I
111		187.07	242.61	15.632	0.050	0.759	0.444	0.866
143		194.50	266.97	15.769 ::		-0.206 ::	-0.179 ::	0.592 ::
36		352.03	256.73	15.779		1.039	0.505	1.000
128		133.63	7.67	15.790	0.160 :	0.778	0.660	1.053
21		127.16	232.02	15.832	0.382	0.976	0.543	1.034
4		238.69	146.67	15.858	0.711 ::	1.359	0.716	1.542
23		157.68	243.29	15.866		1.364	0.803	1.527
92		412.02	252.96	15.872	0.296	0.877	0.527	1.011
57		170.38	118.58	15.889		0.993	0.585	1.088
80		485.76	236.36	15.892	0.433 :	1.024	0.549	1.176
65		308.61	107.52	15.903	0.340	0.921	0.485	0.987
88		343.82	171.77	15.975	0.216	0.818	0.459	0.915
76		465.26	272.99	16.037	0.619 :	1.000	0.549	1.116
131		496.09	374.78	16.041	0.399 ::	0.994	0.587	1.118
110		7.09	87.70	16.114	0.206	1.011	0.604	1.215
25		179.29	157.11	16.115	0.204 :	0.912	0.513	1.058
40		367.93	411.73	16.153	0.257 :	1.033	0.517	1.124
130		322.10	340.83	16.189	0.406 :	0.918	0.719	0.989
52		131.25	63.93	16.214	0.701 ::	2.002	1.051	2.112
70		393.44	236.29	16.232		1.053	0.597	1.105
44		413.35	194.65	16.248	0.473 :	0.891	0.509	1.000
59		193.7	221.56	16.252	0.246 :	0.785	0.547	1.054
106		416.26	211.01	16.279	0.361 :	1.059	0.630	1.147
120		499.71	482.31	16.308	0.499 ::	1.129	0.513	1.099
113		226.53	17.30	16.335		1.199	0.677	1.278
82		211.32	330.55	16.352	0.346 ::	1.001	0.559	1.133
138		254.30	218.71	16.373		1.144	0.673	1.410
24		166.43	133.16	16.386		1.059	0.677	1.295
15		74.76	145.21	16.452	0.498 ::	0.857	0.580	1.077
14		60.17	135.84	16.493		1.566	0.891	1.886
126		100.82	261.05	16.503	0.594 ::	0.934	0.560	1.038
115		6.71	281.54	16.538		1.278	0.641	1.236
156		168.57	401.75	16.565 ::		1.016 ::	0.371 ::	1.150 ::
108		445.07	454.09	16.568		1.527	0.856	1.790
20		122.72	455.01	16.579		1.565	0.817	1.781
83		253.96	335.69	16.669	0.169 :	0.959	0.459	1.095
85		272.67	315.35	16.675	0.471 ::	1.059	0.679	1.407
147		166.95	401.80	16.680		0.972	0.540	1.112
124		472.71	432.65	16.727		1.687	1.010	2.122
95		7.72	176.97	16.730	0.494 ::	0.892	0.635	1.105
133		85.07	437.27	16.784	0.522 ::	1.267 :	0.552 :	1.370
149		70.97	241.03	16.796		1.313 ::	0.575	1.148
22		132.61	337.07	16.805		1.266	0.653	1.358
114		506.67	248.75	16.808		1.020	0.561	1.201
104		326.89	472.73	16.827	0.729 ::	0.848	0.549	1.104
47		57.12	431.64	16.829		1.194	0.712	1.412
69		390.78	471.27	16.859		1.514	0.931	1.865
91		376.23	27.68	16.914		1.169	0.602	1.214
136		214.56	149.66	16.935	1.299 ::	1.029 :	0.769	1.413
150		151.34	331.56	16.955		1.142 :	0.445	1.080
63		229.11	490.58	16.967	0.415 ::	0.999	0.523	1.082
145		259.28	354.31	16.967		0.754 :	0.587	1.380
135		99.85	325.75	17.022		0.692 :	0.591	0.993
29		227.39	105.49	17.048		1.149	0.787	1.415

#	V&F	X	Y	V	U − B	B − V	V − R	V − I
58		180.26	361.39	17.062		1.131	0.578	1.166
144		73.56	144.96	17.099 ::		-0.008 ::	1.308 ::	1.925 ::
142		40.94	268.97	17.161		0.771 :	0.675	1.436
48		66.91	481.84	17.166	0.510 ::	1.092	0.788	1.562
119		493.02	245.52	17.179	0.466 ::	1.072 :	0.567	1.178
109		504.83	363.65	17.185		1.117	0.649	1.335
134		304.79	272.41	17.185		0.227 ::	0.505	0.950
93		463.57	216.78	17.193	-0.370 ::	1.537 :	0.765	1.611
68		369.20	83.22	17.257		0.946	0.756	1.261
98		92.11	64.82	17.308		1.194 :	0.571	1.109
16		76.56	39.01	17.312		1.184	0.689	1.168
146		37.79	58.98	17.332		1.010 ::	0.583 :	1.084 :
45		423.71	327.30	17.335		1.178 :	0.548	1.262
26		190.41	55.51	17.341	0.450 ::	0.984	0.506	1.052
42		392.94	149.75	17.351		1.296 :	0.655	1.413
56		151.45	396.92	17.376	-0.410 ::	1.088 :	0.588	1.170
132		351.52	7.77	17.395		1.208	0.513	1.217
152		378.90	327.60	17.397		0.898 ::	-0.092 :	1.252
64		287.24	51.57	17.406		1.030	0.612	1.287
94		486.97	274.22	17.468		1.033 :	0.492	1.110
99		211.01	320.00	17.496		0.918	0.604	1.117
148		394.82	433.01	17.539		1.222 ::	0.789 :	1.420 :
153		101.15	315.26	17.540		0.917 ::	-0.092 :	1.122 :
30		256.79	94.85	17.558		1.439 :	0.606	1.359
96		11.13	219.47	17.591		1.039 :	0.594	1.261
53		134.47	310.72	17.600		1.489 ::	0.715	1.491
61		215.97	169.72	17.617	0.765 ::	1.055 :	0.605	1.376
112		189.69	208.72	17.714		1.336 ::	0.680	1.426
97		80.11	384.54	17.724		2.029 ::	1.455	2.790
31		273.01	338.68	17.747		1.039 :	0.729	1.339
127		132.66	197.08	17.763		1.561 ::	0.456 :	1.218 :
123		373.94	215.27	17.836		1.393 ::	0.974	1.762
87		316.64	29.68	17.868		1.326 ::	0.794 :	1.817 :
74		453.86	71.18	17.953		1.320 ::	0.694 :	1.618
50		80.30	168.84	17.966		0.980 ::	0.737 :	1.479
39		364.60	121.54	18.027		1.720 ::	0.713 :	1.215
155		445.44	432.89	18.041 ::		1.407 ::	0.666 ::	1.488 ::
107		427.00	478.45	18.194 :		1.141 ::	0.632 ::	1.363 :
139		482.84	393.23	18.234 ::		1.591 ::	0.954 ::	1.655 ::
67		322.76	23.27	18.342 :		1.006 ::	0.950 ::	1.850 :
118		400.03	87.39	18.385 ::		1.484 ::	0.493 ::	1.197 ::
46		478.63	368.66	18.468 :		0.694 ::	0.968 :	1.755 :
62		219.24	431.68	18.620 :		1.042 ::	0.596 ::	1.513 ::

Table 4. Intrinsic colours and magnitudes

#	V_0	$(U-B)_0$	E_{U-B}	$(B-V)_0$	E_{B-V}	M_V	$LogT_{\rm eff}$	$Log(L/L_\odot)$	$M/M_\odot$	Note	S.T.
100	7.26	-0.98	0.36	-0.27	0.49	-4.64	4.43	4.91	18.75		B0IV
81	7.81	-1.09	0.49	-0.30	0.65	-4.09	4.50	4.83	19.24		B0IV
84	8.07	-1.01	0.39	-0.28	0.52	-3.83	4.45	4.61	15.35		B1IV
49	8.10	-1.04	0.43	-0.29	0.58	-3.80	4.47	4.64	16.32		B0IV
5	9.26	-0.83	0.33	-0.23	0.45	-2.64	4.33	3.86	8.83		
3	9.51	-0.83	0.34	-0.23	0.46	-2.39	4.33	3.77	8.53		
33	10.15	-0.70	0.38	-0.20	0.52	-1.75	4.26	3.36	6.52		
157	10.35	-0.86	0.33	-0.24	0.44	-1.55	4.34	3.46	7.72		B1.5VI
55	10.39	-0.61	0.39	-0.17	0.52	-1.51	4.20	3.12	5.46		
7	10.62	-0.18		-0.06		-1.28	4.10	2.74	3.98	pm	
17	10.88	-0.72	0.38	-0.20	0.51	-1.02	4.28	3.10	6.04		
19	11.11	-0.54	0.40	-0.15	0.53	-0.79	4.15	2.71	4.35		
60	11.20	-0.65	0.39	-0.18	0.53	-0.70	4.23	2.86	5.10		
27	11.43	-0.45	0.36	-0.13	0.48	-0.47	4.12	2.50	3.84		
34	11.45	-0.53	0.44	-0.15	0.58	-0.45	4.15	2.57	4.10		
9	11.55	-0.56	0.38	-0.16	0.51	-0.35	4.17	2.58	4.20		
129	11.57	-0.50	0.38	-0.14	0.51	-0.33	4.14	2.49	3.92		
51	11.74	-0.50	0.33	-0.14	0.45	-0.16	4.13	2.42	3.79		
10	11.76	-0.52	0.38	-0.15	0.51	-0.14	4.15	2.44	3.88		
101	11.81	-0.56	0.38	-0.16	0.50	-0.09	4.17	2.47	4.05		
18	12.34	-0.10	0.46	-0.03	0.62	0.44	3.99	1.87	2.64		
1	12.47	-0.27	0.38	-0.08	0.51	0.57	4.04	1.91	2.80		
28	12.48	-0.29	0.38	-0.09	0.51	0.58	4.05	1.93	2.84		
158	12.50	-0.29	0.38	-0.09	0.51	0.60	4.05	1.92	2.83		
2	12.62	-0.17	0.37	-0.05	0.50	0.72	4.01	1.79	2.59		
32	12.77	-0.15	0.47	-0.05	0.63	0.87	4.00	1.72	2.52		
125	12.83	-0.16	0.47	-0.05	0.62	0.93	4.00	1.70	2.50		
11	13.00	-0.12	0.48	-0.04	0.64	1.10	4.00	1.61	2.39		
73	13.03	-0.15	0.51	-0.05	0.68	1.13	4.00	1.61	2.41		
54	13.19	-0.20	0.57	-0.06	0.76	1.29	4.01	1.57	2.44		
122	13.21	-0.15	0.50	-0.05	0.66	1.31	4.00	1.54	2.37		
154	13.34	0.06		0.01		1.44	3.97	1.42	2.17		
89	13.53	0.03		0.35		1.63	3.84	1.29	1.88	pm	
105	13.69	0.11		0.12		1.79	3.93	1.25	1.95		
137	13.79	0.01		0.34		1.89	3.84	1.19	1.79	pm	
36	14.19			0.53		2.29	3.79	1.05	1.52	pm	
21	14.24	-0.00		0.46		2.34	3.80	1.02	1.62	pm	
57	14.30			0.48		2.40	3.80	1.00	1.60	pm	
80	14.30	0.05		0.51		2.40	3.79	1.00	1.60	pm	
76	14.44			0.49		2.54	3.80	0.94	1.56	pm	
131	14.45	0.02		0.48		2.55	3.80	0.94	1.55	pm	
130	14.60	0.02		0.40		2.70	3.82	0.87	1.52		
70	14.64			0.54		2.74	3.79	0.87	1.49	pm	
44	14.66	0.09		0.38		2.76	3.83	0.85	1.53		
120	14.72	0.12		0.62		2.82	3.77	0.85	1.36	pm	
15	14.86	0.11		0.34		2.96	3.84	0.76	1.54		
156	14.97			0.50		3.07	3.80	0.73	1.40	pm	
85	15.08	0.09		0.55		3.18	3.79	0.69	1.37	pm	
147	15.09			0.46		3.19	3.81	0.68	1.39		
95	15.14	0.11		0.38		3.24	3.83	0.65	1.50		
133	15.19	0.14		0.75		3.29	3.74	0.69	1.26	pm	
114	15.22			0.51		3.32	3.79	0.64	1.34		
91	15.32			0.66		3.42	3.76	0.61	1.29	pm	
63	15.37	0.03		0.49		3.47	3.80	0.57	1.33		

Table 4. continued

#	V_0	$(U-B)_0$	E_{U-B}	$(B-V)_0$	E_{B-V}	M_V	$Log T_{eff}$	$Log(L/L_{\odot})$	$M/M_{\odot}$	Note	S.T.
58	15.47			0.62		3.57	3.77	0.55	1.26	pm	
48	15.57	0.13		0.58		3.67	3.78	0.50	1.25		
119	15.59	0.08		0.56		3.69	3.78	0.49	1.25		
109	15.59			0.60		3.69	3.77	0.50	1.24	pm	
68	15.66			0.43		3.76	3.81	0.45	1.44		
16	15.72			0.67		3.82	3.76	0.46	1.13	pm	
146	15.74			0.50		3.84	3.80	0.43	1.29	pm	
26	15.75	0.07		0.47		3.85	3.80	0.42	1.33		
132	15.80			0.69		3.90	3.76	0.43	1.10	pm	
152	15.80			0.38		3.90	3.83	0.39	1.57	pm	
64	15.81			0.52		3.91	3.79	0.40	1.26		
94	15.88			0.52		3.98	3.79	0.37	1.26	pm	
99	15.90			0.40		4.00	3.82	0.35	1.30		
148	15.95			0.71		4.05	3.75	0.38	1.06	pm	
153	15.95			0.40		4.05	3.82	0.33	1.30	pm	
96	16.00			0.53		4.10	3.79	0.33	1.24	pm	
31	16.15			0.53		4.25	3.79	0.26	1.24	pm	
74	16.36			0.81		4.46	3.73	0.23	0.98	pm	
155	16.45			0.89		4.55	3.70	0.23	0.98	pm	
107	16.60			0.63		4.70	3.77	0.10	1.10	pm	

Note: pm = possible member.
MK Spectral types are from FitzGerald *et al* (1979).
Remark: Star #100 = HD126449;
Star # 84 = -59.5577;
Star # 81 = -59.5580;
Star # 49 = -59.5579;
Star # 3 = IDS 14204S5911A = LSS 3241;
Star # 43 = -59.5574;
Star # 33 = IDS14204S5011E.